Correlation of the concentration of the carbon-associated radiation damage levels with the total carbon concentration in silicon

G. Ferenczi, C. A. Londos,[a] T. Pavelka, and M. Somogyi
Research Institute for Technical Physics of the HAS, 1325 Budapest, Ujpest 1, P. O. Box 76, Hungary

A. Mertens
Bereich 06, Sektion Physik, Humboldt Universitat, Berlin, German Democratic Republic

(Received 8 April 1987; accepted for publication 2 September 1987)

The dominant carbon-related radiation damage center in silicon was studied in detail by deep level transient spectroscopy. Samples with different carbon and oxygen content were implanted with gradually increasing proton fluence. Two energetically closely spaced levels were revealed and tentative identities were assigned. One at $E_T + E_V = 0.344$ eV ($\sigma_p = 1.1\times 10^{-16}$ cm^2) is assigned as the $C + O_i$ complex, and that at $E_T + E_V = 0.370$ eV ($\sigma_p = 8\times 10^{-18}$ cm^2) is assigned as the C_s-Si_i-C_s complex. It was shown that the concentration of these defects is correlated to the total concentration of carbon in the crystal.

I. INTRODUCTION

The yield and properties of very large scale integration (VLSI) devices which are mainly fabricated on Czochralski (CZ) silicon wafers are significantly influenced by the behavior of oxygen in the silicon substrates. It is well established[1,2] that the presence of carbon in the silicon lattice significantly influences the precipitation properties of oxygen acting as a nucleation site. It is argued[1] that low carbon concentration is favorable. The widely used IR absorption technique cannot usually detect carbon concentrations below 1×10^{16} cm^{-3} on samples with standard wafer thickness. Alternative ways to detect low carbon concentrations would therefore be welcome.

One possibility is offered by the fact that some of the radiation-induced defects are related to the carbon and oxygen impurities already present in the host silicon lattice. Measuring the electronic and vibronic bands of these defects, Davies *et al.*[3] have suggested that, by measuring the electronic absorption on the carbon related radiation damage centers, the overall carbon concentration can be assessed down to $[C_s] \simeq 10^{15}$ cm^{-3}.

Hall-effect and space-charge spectroscopy techniques are generally more sensitive than optical techniques for the detection of minute amounts of electrically active impurities in semiconductors. The carbon- and oxygen-related defects are easily detected by these techniques.[4–11]

In this work, we intend to concentrate on a carbon-related level usually reported with $E_V + E_T = 0.36$ eV, which forms around room temperature and anneals out around 300–350 °C. This defect was first described more than 20 years ago,[12] but its identity is still subject to controversy; candidates are COV_2 or C_i-C_s (recently[13] corrected as C_s-Si_i-C_s). The intention of this paper is to resolve this long-standing controversy which may open the way to use DLTS data for the measurement of the overall carbon concentration in silicon.

[a] Permanent address: University of Athens, Physics Department, Solid State Section, 104 Solonos Street, Athens, Greece.

II. EXPERIMENT

10–15 Ω cm, B-doped, *p*-type silicon materials were used. Three groups of samples were selected (Table I). Schottky contacts were prepared by Ag^+ implantation (10 keV, 5×10^{16} cm^{-2}) as described in Ref. 14. Subsequently, the samples were implanted with 300-keV H^+ at room temperature using varying fluence levels between (4×10^9–6×10^{10}) cm^{-2}. DLTS measurements were performed with a high-sensitivity lock-in type spectrometer DLS-82E, manufactured by Semitrap, Hungary.

In the course of this work, we made use of the special features of this spectrometer which—for the sake of clarity—are summarized here: the spectrometer uses the symmetrical square wave weight function of a broadband lock-in amplifier to average the capacitance transients.[15] The capacitance signal is gated off during the filling pulse and a hold period immediately following the pulse. The minimum length of this hold period is determined by the response time of the capacitance meter. The lock-in is synchronized in such a way that the averaging of the transients commences after the hold period ends [see Figs. 1(a) and 1(b)]. The length of the hold period is kept as a constant portion of the repetition period time. Hence, the phase of the lock-in is kept constant, independent of the repetition frequency of the lock-in. The capacitance meter is gated off again in the middle of the measuring cycle which is followed by another hold period.

TABLE I. The three groups of samples used in this work.

	Float zone (FZ)	$Czochralski_{low\,C}$	$Czochralski_{high\,C}$
$N_{O_i}\times 10^{16}$ (cm^{-3})	<1	50	50
$N_{C_s}\times 10^{16}$ (cm^{-3})	1	0.8	5

 0021-8979/88/010183-07$02.40 © 1987 American Institute of Physics

Downloaded 24 Sep 2009 to 195.134.94.40. Redistribution subject to AIP license or copyright; see http://jap.aip.org/jap/copyright.jsp

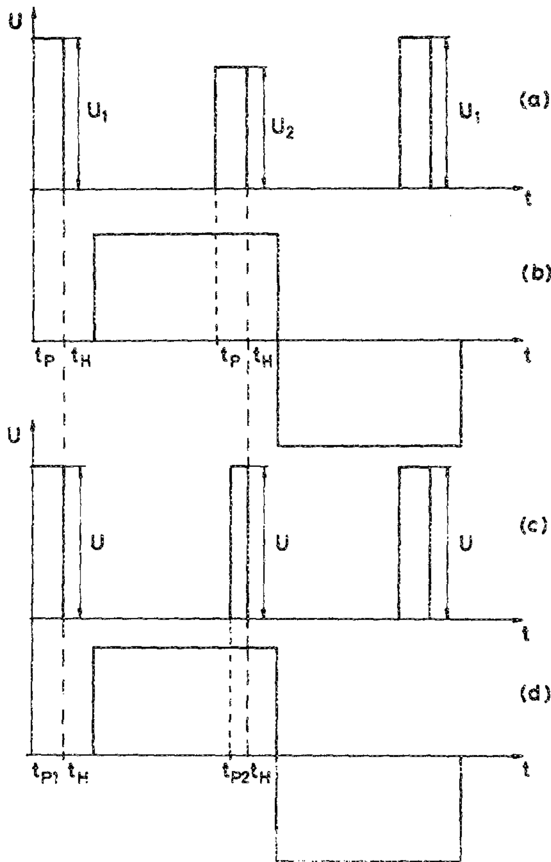

FIG. 1. (a) Filling pulse sequence used for depth profiling of deep levels: the widths of the pulses are equal, the amplitude difference determines the spatial resolution. (b) The symmetrical wave weight function of the lock-in, with t_H as the hold period which is a constant portion of the repetition time. (c) Filling pulse sequence used for separating the thermal emission transients from traps with different capture cross sections. The amplitudes are equal, the pulse widths are different. (d) The timing of the lock-in reference function is the same as in case (b). It has to be pointed out that the position in time of the falling edge of the shorter filling pulse is kept constant relative to the weight function of the lock-in.

This enables us to insert a second filling pulse as seen in Figs. 1(a) and 1(c). This differential DLTS approach[16] is used for depth profiling [Fig. 1(a)] and for peak separation [Fig. 1(c)]. The repetition frequency of the lock-in may be scanned continuously, which makes DLTS measurements possible at constant temperatures. This so-called isothermal frequency scan DLTS technique[17] is used extensively throughout this paper.

III. EXPERIMENTAL RESULTS ON THE RADIATION DAMAGE LEVELS

A typical temperature-scan, majority-carrier DLTS spectrum of a H^+-implanted, *p*-type Si sample is illustrated in Fig. 2. The peak labeled H_0 is due to some unidentified defect present in the material before implantation. The peaks labeled H_1–H_6 are implantation-induced defects present with fluence-dependent intensities in all samples investigated here. These defects were carefully analyzed, and the results are summarized in Table II. As seen, the majority of these defects were previously described and identified.

A few remarks are, however, noteworthy:

(i) The peak labeled H_2 is identified as $C_i(0/+)$. It is known that the carbon interstitials are mobile at room temperature,[5] where the implantation was done, and react with other defects to form H_4.[4–8] This reaction is rather slow at room temperature and the samples were kept at -18 °C after implantation until the measurement. Annealing the sample at 100 °C for 20 min reduced the concentration of H_2 while the concentration of H_4 increased in agreement with previous observations.[8]

(ii) The peak labeled H_3 has not been reported previously. Irmscher[4] reports a peak labeled H_3' appearing at a temperature similar to H_3. H_3' disappears[4] upon annealing, however, while H_3 remains stable. It has to be noted that one can easily separate H_3 in the traditional temperature-scan DLTS only in FZ materials at low-proton fluence levels, as illustrated in Fig. 3. In CZ samples even at relatively low fluence levels, H_3 appears an insignificant shoulder on the temperature-scan spectra. Since the introduction rate of H_3 is lower than that of H_4, the contribution of H_3 to the H_4 peak is fluence dependent.

(iii) For the identification of H_5 we accepted the identification by Irmscher,[4] who suggests that H_5 is the complex of radiation-induced vacancy with an unspecified impurity.

(iv) H_6 appears to be a characteristic mid-gap level.[18] To gain insight into the origin of H_4, the introduction rate of this defect in different samples was studied. While the intro-

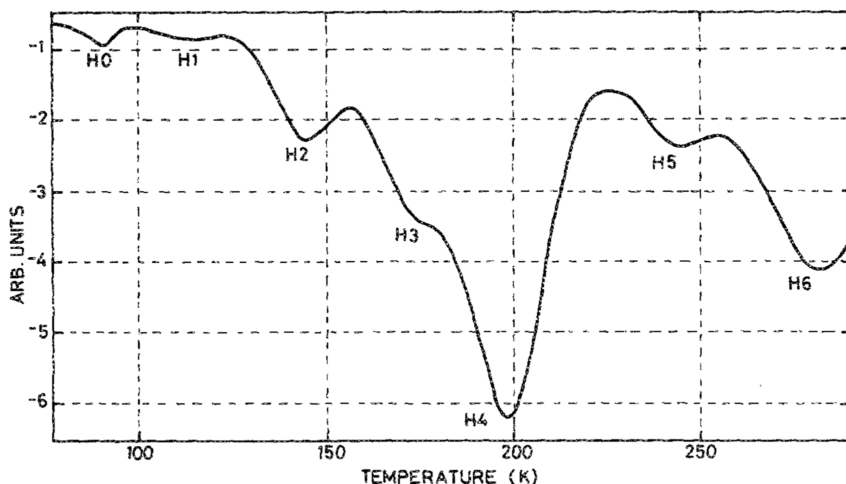

FIG. 2. Temperature-scan DLTS recording of the majority-carrier peaks of a float-zone silicon wafer implanted with 300-keV H^+ at room temperature; fluence level: 4×10^{10} cm^{-2}; $e_{max} = 67$ s^{-1}.

Downloaded 24 Sep 2009 to 195.134.94.40. Redistribution subject to AIP license or copyright; see http://jap.aip.org/jap/copyright.jsp

TABLE II. Observed radiation damage centers due to proton irradiation.

Defects	H_1	H_2	H_3	H_4	H_5	H_6
T_{max} K at $e_p = 67\ s^{-1}$	117	144	174	198	238	281
$E_V + E_T$ (eV) This work	0.19	0.27	0.279	0.35[a]	0.52	0.55
$E_V + E_T$ (eV) Published previously	0.18–023	0.28–0.30	···	0.33–0.38	0.48–0.53	b
References	4–10	4–9	···	4–10	4,7,10	4
Identification	$V_2(0/+)$	$C_i(0/+)$	?	COV_2 or[c] C_i-C_s	VY	?

[a] Average value. For detailed analysis see the analysis of H_4 in Sec. IV.
[b] A similar peak was reported previously (Ref. 4), but no activation energy was given.
[c] For details of the identification, see Sec. V.

duction rate of the other radiation-induced defects listed in Table II are similar in all the samples investigated in this study, H_4 behaves markedly differently. To make this statement more quantitative, the fluence and sample dependence of the introduction rate of H_4 is illustrated in Fig. 4. In the FZ samples with low C and O concentrations, the introduction rate of H_4 is not significantly larger than that of the other radiation-induced defects. The introduction rate in the $CZ_{low\,C}$ and in the $CZ_{high\,C}$ samples increases by more than a factor of 3. These data suggest that—in agreement with previous attempts of identification[4–11]—both carbon and oxygen contribute to the formation of H_4. In Sec. IV we try to clarify how this actually happens.

IV. DETAILED DLTS ANALYSIS OF H_4

The Schottky barriers on the samples investigated in this work were prepared by low-energy, high-fluence Ag^+ implantation without annealing. The thickness of the amorphous layer beneath the metallization is estimated[14] to be around 10 nm, which does not influence the electrical properties of the junction. Depth profiling of the H_4 level using the differential DLTS approach[16] [see Figs. 1(a) and 1(b)] revealed that H_4 is formed as a result of both the proton implantation and the Ag^+ implantation, as seen in Fig. 5. The proton-induced peak is centered at 2.7 μm, in good agreement with the theoretically predicted value calculated for the spatial distribution of that portion of the incident ion energy which is deposited in the lattice into atomic processes.[19] H_4 is also produced by the recoil cascade resulting from the Ag^+ implantation in the vicinity of the surface layer. The same depth distribution was observed for the other radiation damage levels H_1–H_6 as well.

We concentrated only on the proton-induced defect. The double-peaked, highly inhomogeneous distribution of H_4 helped us to eliminate the influence of the edge layer on the capture cross-section measurements. The amplitude of the filling pulse was selected to reach a relatively defect-free part of the space-charge layer (typically, the width of the

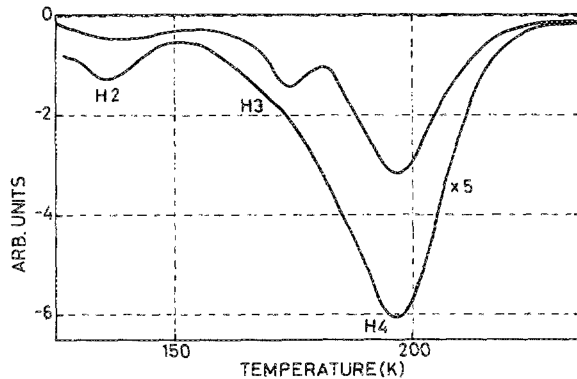

FIG. 3. Temperature-scan DLTS spectra at $e_{max} = 67\ s^{-1}$. Upper trace: recorded on FZ material; proton fluence: $4\times10^9\ cm^{-2}$. Lower trace: recorded on a $CZ_{low\,C}$ material; proton fluence: $1\times10^{10}\ cm^{-2}$.

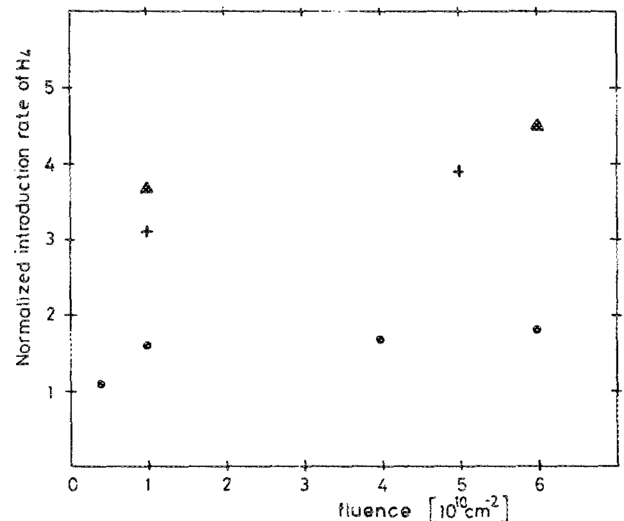

FIG. 4. Normalized introduction rate of H_4. The averaged introduction rates of H_1, H_3, H_5, and H_6 were used as normalization factor. FZ: ●; $CZ_{low\,C}$: +; $CZ_{high\,C}$: ▲.

Downloaded 24 Sep 2009 to 195.134.94.40. Redistribution subject to AIP license or copyright; see http://jap.aip.org/jap/copyright.jsp

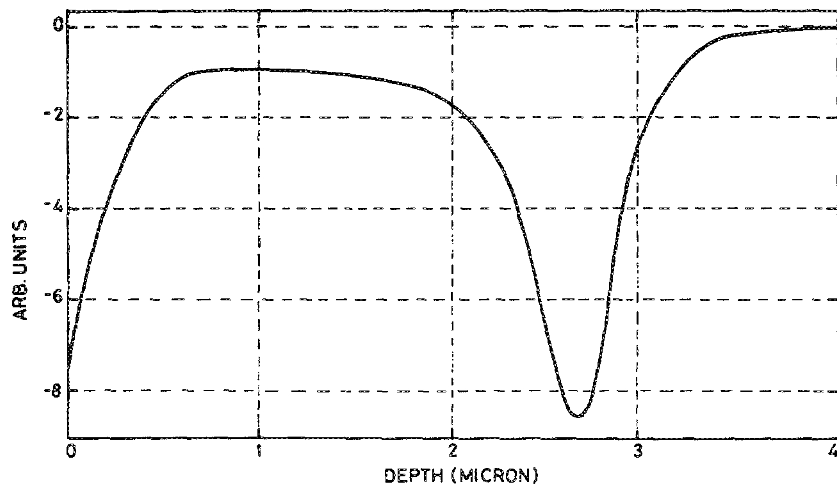

FIG. 5. Depth profile measured in the differential DLTS mode at $T = 195$ K; $e_{max} = 67$ s^{-1} on a $CZ_{low C}$ sample.

space-charge layer was reduced to 0.8 μm and then increased again up to 4 μm). In this way, the inhomogeneous filling of the traps due to the free-carrier tail and its influence on the capture cross section measurement was strongly reduced. On the majority of the samples, two clearly distinguishable capture cross sections were measured, as seen in Figs. 6(a) and 6(b). It is worthwhile to mention that the capture cross-section measurements in Fig. 6(a), which are performed in the frequency-scan mode, clearly resolve the peak labeled H_3. This is mainly due to the superior energy resolution of the frequency scan technique. (To achieve equivalent energy resolution with a temperature scan, significant data points

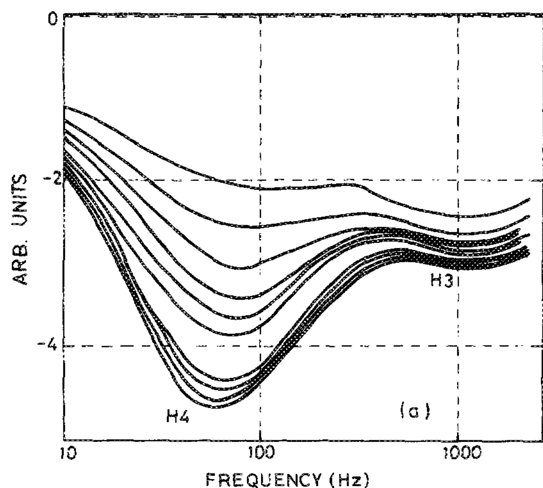

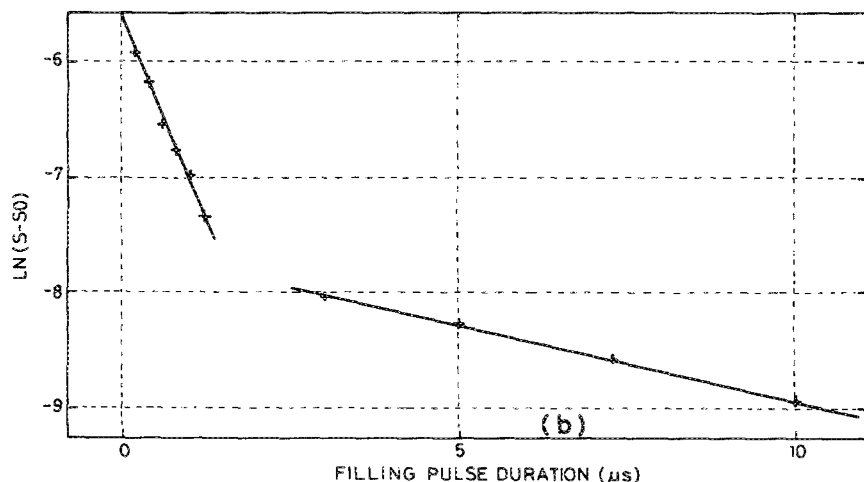

FIG. 6. (a) Series of capture cross-section measurements performed in the frequency scan mode on the proton-induced H_4 level at 200 K. (Sample: FZ; proton fluence: 1×10^{10} cm^{-2}.) (b) The corresponding evaluation of the two capture cross sections measured for H_4. S_0 is the DLTS signal amplitude when the trap is saturated, and S is the DLTS signal amplitude at the different pulse duration.

Downloaded 24 Sep 2009 to 195.134.94.40. Redistribution subject to AIP license or copyright; see http://jap.aip.org/jap/copyright.jsp

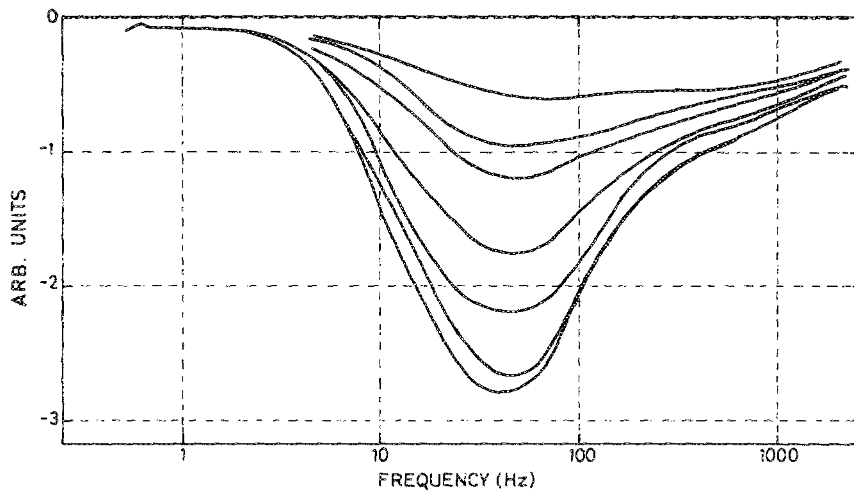

FIG. 7. Series of capture cross-section measurements performed in the frequency scan mode on the proton-induced H_4 level at 195 K. (Sample: $CZ_{low\,C}$; proton fluence: $5\times10^{10}\,cm^{-2}$.)

should be recorded at every 0.04 K.) The values of the two capture cross sections of the H_4 peak averaged over eight different samples are

$$\sigma_{p_{H_4\,fast}} = (1.1 \pm 0.1)\times10^{-16}\,cm^2\,,$$

$$\sigma_{p_{H_4\,low}} = (8 \pm 2)\times10^{-18}\,cm^2\,.$$

For completeness, the capture cross section of H_3 is

$$\sigma_{p_{H_3}} = 2.7\times10^{-16}\,cm^2\,.$$

The H_4 level induced by the highest fluence proton implantation on the $CZ_{low\,C}$ sample dominantly contained only the fast component as seen in Fig. 7, which is to be compared to Fig. 6(a).

At this point, it was crucial to decide whether the two components of the capture process originate from the same defect or we are dealing with two different species. The pulse sequence in Fig. 1(c) was used. The width of the first pulse was long enough to fill both components while the second pulse could fill only the fast component. Multiplication of these transients with the weight function of Fig. 1(d) would yield an output containing information only on the slow component. With the use of this pulse sequence, frequency-scan measurements were performed at six different constant temperatures, as shown in Fig. 8, to determine the activation energy of the slow component of H_4.

Alternatively, using a single filling pulse short enough to fill only the faster component, the activation energy of the fast component can be determined independently. The results are summarized in Fig. 9, which—for completeness—contains the Arrhenius plot for H_3 as well. The measured activation energies (averaged over eight samples) are

$$(E_V + E_T)_{H_4\,fast} = (0.344 \pm 006)\ eV\,,$$

$$(E_V + E_T)_{H_4\,slow} = (0.370 \pm 0.002)\ eV\,.$$

For completeness, the activation energy of H_3 is

$$(E_V + E_T)_{H_3} = 0.28\ eV\,.$$

The accuracy of the measured data (captured cross section and activation energy) is due to the thermal equilibrium achieved during frequency scan. The peak separation technique described previously allows the determination of the concentration of the individual components of H_4 as well.

We can safely state that H_4 consists of two energetically closely spaced components with different activation energies and capture cross sections. The improved experimental technique used in this work allowed us to resolve these states for the first time. The concentration of the individual components of H_4 as a function of the proton fluence is tabulated in Table III.

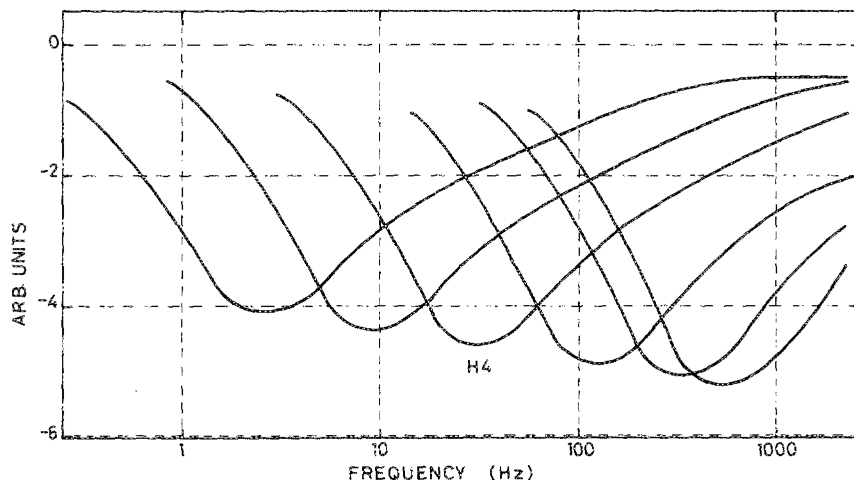

FIG. 8. Series of frequency scan spectra measured at six different temperatures using the double-pulse technique. (Sample: $CZ_{high\,C}$; proton fluence: $6\times10^{10}\,cm^{-2}$.)

Downloaded 24 Sep 2009 to 195.134.94.40. Redistribution subject to AIP license or copyright; see http://jap.aip.org/jap/copyright.jsp

TABLE III. Proton fluence dependence of the components of H_4.

Sample	FZ		$CZ_{low\,C}$		$CZ_{high\,C}$	
Fluence $\times 10^{10}$ (cm^{-2})	fast $\times 10^{12}$ (cm^{-3})	slow $\times 10^{12}$ (cm^{-3})	fast $\times 10^{12}$ (cm^{-3})	slow $\times 10^{12}$ (cm^{-3})	fast $\times 10^{12}$ (cm^{-3})	slow $\times 10^{12}$ (cm^{-3})
0.4	2.3	0.26	...	...	...	...
1	9.5	1.3	5.6	0.8	30	2.9
4	17	2.3	...	...	...	...
5	...	...	32	1.6[a]	...	...
6	23	4.8	...	...	140	22

[a] Estimated value, less accurate than the rest of the data.

V. DISCUSSION

Previous works[4-11] identified H_4 either as the COV_2 complex[20] or the C_i-C_s complex,[21] which was later corrected to the C_s-Si_i-C_s complex.[13] In the previous section, it was shown for the first time that H_4, in fact, consists of two different species. We identify the fast component of H_4 as the COV_2 complex or the $C + O_i$ complex according to Ref. 3 and the slow component as the C_s-Si_i-C_s complex. These assignments are supported by the fact that both defects are formed around room temperature by means of the mobile carbon interstitials.[5]

As seen qualitatively from Table III, the concentration of the slow component increases strongly and monotonically with increasing carbon concentration of the sample and is independent of the oxygen content. On the other hand, the concentration of the fast component depends on both the variation of the oxygen and carbon content of the sample (see, e.g., the highest fluence data for the fast components for the three different sets of samples). With the assumption that the C_i atoms interact only with C_s or the VO complex, the results of Table III make our identification probable.

The previous statements can be made more quantitative. Normalization of the measured concentration values of the C_s-Si_i-C_s complex by the total carbon concentration of the samples (the carbon concentrations as listed in Table I were measured on thicker wafers from the same ingot for the FZ samples and for the $CZ_{low\,C}$ samples), gives the fluence dependence illustrated in Fig. 10. The uncertainty in the determination of the actual carbon concentration of the DLTS samples is responsible for the large scatter of the data.

The observed fluence dependence of the carbon complex is independent of the carbon concentration of the sample. This indicates that, at any given irradiation fluence, the concentration of the C_s-Si_i-C_s complex is a well defined function of the total carbon concentration of the sample. This is illustrated in Fig. 11. Since the carbon concentration range of our samples is very limited, an accurate determination of the functional dependence could not be established.

VI. CONCLUSIONS

A new insight into the long-standing controversy concerning the nature of the dominant carbon related radiation damage level in silicon has been suggested. It was established that this level labeled as H_4 throughout this paper, in fact consists of two states closely spaced in energy. The ratio of the two components depends on the relative oxygen over carbon concentration ratio in the crystal and on the implantation dose. The double-pulse technique proposed in this paper is capable of separating the two components of H_4.

By selecting a series of samples with different carbon concentration, the functional dependence of the C_s-Si_i-C_s defect concentration on the initial carbon concentration may

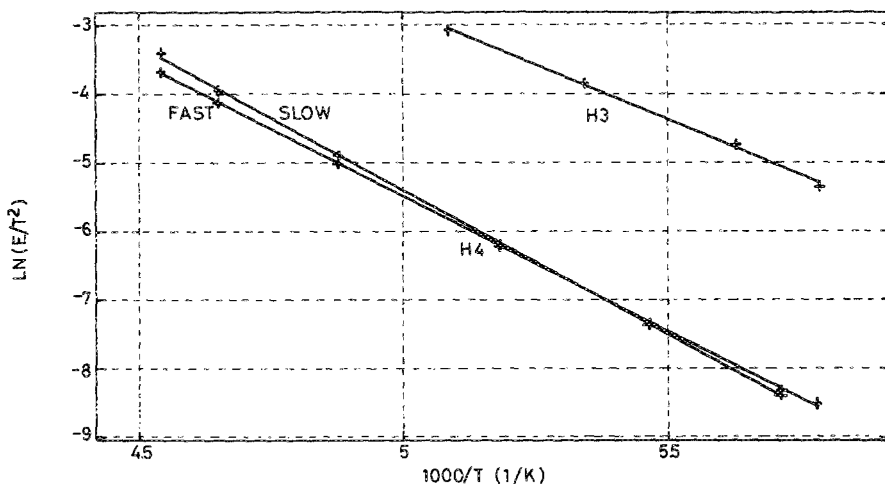

FIG. 9. Arrhenius plots of the two components of H_4 and of H_3 derived from frequency scan measurements. (Sample: $CZ_{high\,C}$; proton fluence: 6×10^{10} cm^{-2}.)

Downloaded 24 Sep 2009 to 195.134.94.40. Redistribution subject to AIP license or copyright; see http://jap.aip.org/jap/copyright.jsp

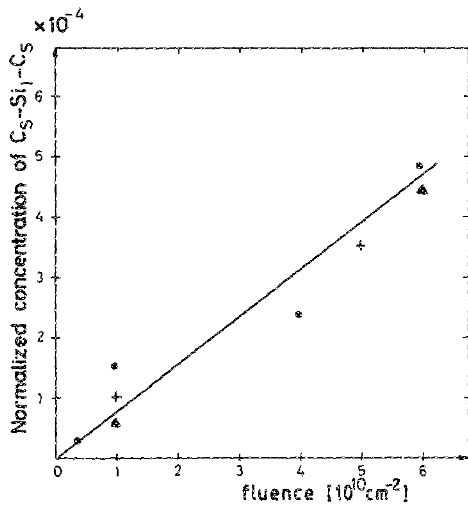

FIG. 10. Proton fluence dependence of the slow components of H_4 normalized by the total carbon concentration of the individual samples: FZ ●; CZ_{low}: +; $CZ_{high\,C}$: ▲.

be established in a similar way as it was done by Davies *et al.*[3] Our initial results illustrated in Fig. 11 are a good indication, that the total carbon concentration may be determined by measuring the concentration of the C_s-Si_i-C_s complex at a given irradiation dose by DLTS. Due to the very high sensitivity of the DLTS technique, it is estimated that the proposed procedure can assess total carbon concentrations down to the $10^{12}/cm^3$ range.

The proposed carbon concentration measurement procedure should be viewed as a next step on the way to use H_4

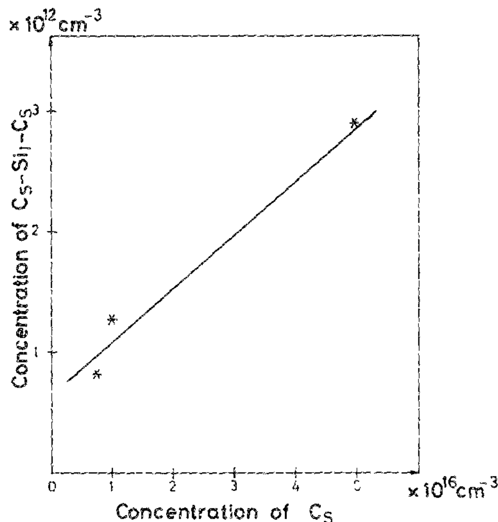

FIG. 11. Dependence of the concentration of the C_s-Si_i-C_s complex on the total carbon concentration at 1×10^{10} cm^{-2} irradiation level.

for determining oxygen and carbon concentration in silicon as was foreseen as a distant possibility by Troxell.[10] The identification of the slow component of H_4 as the C_s-Si_i-C_s complex can find a different application as well.

By using the scanning DLTS technique, the lateral distribution of the C_s-Si_i-C_s complex can be revealed. Correlated with the oxygen precipitation patterns, the role of carbon as a nucleation site for oxygen precipitation might be studied more accurately than was possible until now.

ACKNOWLEDGMENTS

We gratefully acknowledge K. Schmalz for the donation of the $CZ_{high\,C}$ samples, the low-dose implantation by H. Kerkow, and the group of Professor Klose, the IR data by P. Stallhofer and E. Hild. The stay of C.A.L. in Budapest was financed by the Greek-Hungarian Scientific-Technical Governmental Agreement.

[1] M. Kanamori and H. Tsuya, Jpn. J. Appl. Phys. **24**, 557 (1985).
[2] F. Shimura, J. Appl. Phys. **59**, 3251 (1986).
[3] G. D. Davies, A. S. Oates, R. C. Newman, R. Woolley, E. C. Lightowlers, M. J. Birns, and J. G. Wilkes, J. Phys. C **19**, 841 (1986).
[4] K. Irmscher. Ph.D. thesis (Humboldt Universität, Berlin, Germany, 1985).
[5] L. C. Kimerling, P. Blood, and W. M. Gibson, Inst. Phys. Conf. Ser. **46**, 273 (1979).
[6] L. C. Kimerling, Inst. Phys. Conf. Ser. **31**, 221 (1977).
[7] P. M. Mooney, L. J. Cheng, M. Süli, J. D. Gerson, and J. W. Corbett, Phys. Rev. B **15**, 3836 (1977).
[8] Y. H. Lee, L. J. Cheng, J. D. Gerson, P. M. Mooney, and J. W. Corbett, Solid-State Commun. **21**, 109 (1977).
[9] J. W. Walker and C. T. Sah, Phys. Rev. B **7**, 4587 (1973).
[10] J. R. Troxell, Solid State Electron. **26**, 539 (1983).
[11] G. Ferenczi, C. A. Londos, T. Pavelka, M. Somogyi, and A. Mertens, Mater. Sci. Forum **10-12**, 947 (1986).
[12] E. Sonder and L. C. Templeton, J. Appl. Phys. **36**, 1811 (1965).
[13] K. P. O'Donnell, K. M. Lee, and G. D. Watkins, Physica **116B**, 258 (1983).
[14] J. Bollmann, H. Klose, and A. Mertens, Phys. Status Solidi A **97**, K95 (1986).
[15] G. Ferenczi and J. Kiss, Acta Phys. Hung. **50**, 285 (1981).
[16] G. Ferenczi, P. Krispin, and M. Somogyi, J. Appl. Phys. **54**, 3902 (1983).
[17] G. Ferenczi, J. Boda, and T. Pavelka, Phys. Status Solidi A **94**, K119 (1986).
[18] G. Ferenczi, Acta Physica Pol. A **67**, 143 (1985).
[19] D. K. Brice, *Ion Implantation Range and Energy Deposition Distributions* (Plenum, New York, 1975), Vol. 1.
[20] Y. H. Lee, J. W. Corbett, and K. L. Brower, Phys. Status Solidi A **41**, 637 (1977).
[21] K. L. Brower, Phys. Rev. B **9**, 2607 (1975).

Downloaded 24 Sep 2009 to 195.134.94.40. Redistribution subject to AIP license or copyright; see http://jap.aip.org/jap/copyright.jsp